International Journal of Minerals, Metallurgy and Materials
Volume 29, Number 8, August 2022, Page 1570
https://doi.org/10.1007/s12613-021-2264-8

Effects of Nd on microstructure and mechanical properties of as-cast Mg–12Gd–2Zn–*x*Nd–0.4Zr alloys with stacking faults

Lixin Hong[1,2], *Rongxiang Wang*[1,2], *and Xiaobo Zhang*[1,2)✉]

1) School of Materials Science and Engineering, Nanjing Institute of Technology, Nanjing 211167, China
2) Jiangsu Key Laboratory of Advanced Structural Materials and Application Technology, Nanjing 211167, China
(Received: 24 November 2020; revised: 11 January 2021; accepted: 29 January 2021)

Abstract: In order to study the effects of Nd addition on microstructure and mechanical properties of Mg–Gd–Zn–Zr alloys, the microstructure and mechanical properties of the as-cast Mg–12Gd–2Zn–*x*Nd–0.4Zr (*x* = 0, 0.5wt%, and 1wt%) alloys were investigated by using optical microscope, scanning electron microscope, X-ray diffractometer, nano indentation tester, microhardness tester, and tensile testing machine. The results show that the microstructures mainly consist of α-Mg matrix, eutectic phase, and stacking faults. The addition of Nd plays a significant role in grain refinement and uniform microstructure. The tensile yield strength and microhardness increase but the compression yield strength decreases with increasing Nd addition, leading to weakening tension–compression yield asymmetry in reverse of the Mg–12Gd–2Zn–*x*Nd–0.4Zr alloys. The highest ultimate tensile strength (194 MPa) and ultimate compression strength (397 MPa) are obtained with 1wt% Nd addition of the alloy.

Keywords: magnesium alloy; neodymium; microstructure; stacking fault; mechanical properties

1. Introduction

Magnesium (Mg) alloys have shown more and more potentials in aerospace, transportation, and other fields because of their high specific strength, high specific stiffness, and low density that can help to achieve lightweight [1–2]. However, in the actual service process, Mg alloys still have some problems, such as poor plasticity and low absolute yield strength [3]. Therefore, in recent years, many researchers have devoted to optimizing mechanical properties of Mg alloys. At present, the main methods to improve the mechanical properties of cast Mg alloys are alloying [4–5], deformation, and heat treatment [6–8].

Rare earth (RE) elements are favorable alloying elements in Mg alloys which are beneficial to mechanical properties. Y, Gd, and Nd are the common RE elements added in Mg alloys [9–11]. The added RE elements can play a role in strengthening and toughening the alloys due to the solid solution, precipitation, and grain refinement [10–11]. Some Mg–RE–Zn/Ni/Cu [12–17] alloys have long period stacking ordered (LPSO) and/or stacking faults (SFs) structures, which show strong anisotropy, act as strong obstacles against the motion of basal slip, and can even turn the basal slip into kind, and hence further improve the mechanical properties of the Mg alloys [18–19]. Previous studies have proved that Mg–Gd–Zn series alloys exhibit good mechanical properties because of the formation of LPSO structures [20–21] or SFs [22]. SFs have been found in deformed Mg–Er–Zn [23] alloys and Mg–Ho–Zn [24] alloys and they are beneficial to improving mechanical properties by restricting dislocations movement [22]. The maximal solid solubility of Gd in Mg is 23.5wt% [25]. GZ51K, GZ61K, and other alloys with low Gd content have relatively low mechanical properties [11,26], so high Gd concentration should be added into the Mg alloys to obtain significant strengthening effect. The maximal solid solubility of Nd in Mg is 3.6wt% [27], and a small amount of Nd element could have a remarkable strengthening effect. LPSO structure could be commonly formed, but SFs could be rarely found in as-cast Mg–Gd–Zn series alloys [28–29]. It is well known that SFs play a determinative role in the formation of LPSO structure. LPSO may nucleate directly through SFs and the lower SF energy is conducive to the formation of LPSO [30].

Mg alloys have limited slip systems and poor formability at room temperature because of the hexagonal close-packed (HCP) crystal structure. The conventional rolled Mg alloys exhibit poor deformation capacity and strong anisotropy. Therefore, the tensile yield strength (TYS) of the alloys may differ greatly from the compression yield strength (CYS) which is called tension–compression yield asymmetry. Tension–compression yield asymmetry often occurs in deformed Mg alloys [31–32], but sometimes it also generates in as-cast Mg alloys [33]. When the ratio of CYS/TYS is less than 1, the Mg alloys show tension–compression yield asym-

✉ Corresponding author: Xiaobo Zhang E-mail: xbxbzhang2003@163.com, xbzhang@njit.edu.cn

metry. When the ratio is greater than 1, the tension–compression yield asymmetry in reverse occurs in Mg alloys [34]. The obvious tension–compression yield asymmetry is not good for the mechanical properties of the alloys. When the alloy is subjected to the cyclic stress during service, TYS and CYS of the alloy are required to be as close as possible to ensure the stability and safety of the workpiece. Weakening the tension–compression yield asymmetry of Mg alloys has an important effect on the deformation processing of the alloy. The common methods of reducing the tension–compression yield asymmetry of Mg alloys are grain refinement, heat treatment, and alloying [34]. For example, adding elements such as Ho or Zn [24] to Mg alloys can reduce the tension–compression yield asymmetry of the alloys by refining grains and forming SFs.

A few studies have shown that adding a small amount of Nd into Mg–RE alloy can optimize the mechanical properties [35–36]. Therefore, Mg–12Gd–2Zn–0.4Zr alloy was selected as the aim alloy in this work, and minor Nd was added into the alloy to study the effects of Nd on the microstructure and mechanical properties of the alloys.

2. Experimental

The nominal Mg–12Gd–2Zn–*x*Nd–0.4Zr alloys (x = 0, 0.5wt%, and 1wt%, denoted as Alloy 1, Alloy 2, and Alloy 3, respectively) were prepared by traditional gravity casting with the raw materials of highly pure Mg (99.99%), Zn (99.99%), and Mg–30wt%Gd, Mg–30wt%Zr, and Mg–30wt%Nd master alloys in an electric resistance furnace. Pure Mg was melted in the steel crucible under a mixed protective atmosphere of CO_2 and SF_6 with the volume ratio of 19:1. Mg–30wt%Gd, Mg–30wt%Nd (only for Alloys 2 and 3), pure Zn, and Mg–30wt%Zr were successively added into molten Mg at 760°C. The melt was stirred for 5 min to homogenize, stabilized for 20 min, and then poured into preheated mold at 720°C. Finally, the ingots were cooled by water.

The microstructures of the as-cast alloys were observed using an optical microscope (OM, OLYMPLUS GX51), a scanning electron microscope (SEM, JSM-6360LV) equipped with an energy dispersive spectrometer (EDS, GENESIS 2000XM60), and a transmission electron microscope (TEM, FEI Tecnai G2 F20). Thin foil with thickness of ~80 μm was punched to discs with diameter of 3 mm, and then the discs were polished by twin-jet electropolishing device (Struers TenuPol-5) with 50 V at −45°C, finally, they were ion thinned for TEM observation. The volume fraction of eutectic phase and grain size were measured by Image-Pro-Plus 6.0 software. The phases of the alloys were analyzed by using an X-ray diffraction (XRD, Rigaku Ultima-IV) with Cu target. The operating voltage was 40 kV and the scanning angle ranged from 20° to 80° with a scanning speed of 6°/min.

Tensile and compression properties of the alloys were evaluated with an electronic material testing machine (Zwick/Roell Z030TH) at room temperature. The gauge length, width, and thickness of the sheet tensile specimen are 15 mm, 3.5 mm, and 1.8 mm respectively. The size of the compression sample is ϕ8 mm × 12 mm. To exhibit better reproducibility, three samples were tested with the tensile and compression speed of 1 mm/min. The fracture morphologies were observed by SEM. Nanohardness of the phases were tested by the nanoindentation tester (Agilent G200) at room temperature with Berkovich-type diamond indenter. The applied load, the rate of increasing load, and the dwell time were 25 mN, 5 mN/s, and 10 s, respectively, and the unloading rate is 100%. At least 10 points were conducted for each phase in the alloys and then took an average value. Microhardness of the α-Mg matrix was tested by Vickers hardness tester (FM-700). The loading was 4.9 N and the dwell time was 15 s. 10 points were measured for each sample to obtain average data.

3. Results and discussion

3.1. Microstructures and phases

Fig. 1 shows the microstructures of the as-cast Mg–12Gd–2Zn–*x*Nd–0.4Zr alloys. They are mainly composed of α-Mg matrix, eutectic phase, and lamellar structures distributed at the matrix grains. The eutectic phase has a discontinuous mesh distribution along the grain boundaries. Some studies have shown that the addition of Nd in Mg alloys can refine

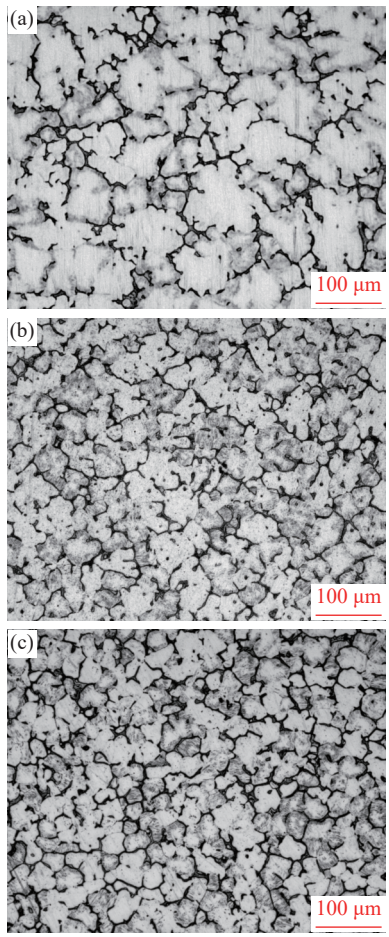

Fig. 1. Optical micrographs of the as-cast alloys: (a) Alloy 1; (b) Alloy 2; (c) Alloy 3.

and uniform the microstructures [36–37]. The volume fractions of eutectic phases of Alloys 1, 2, and 3 are 5.7%, 11.1% and 14.3%, respectively. Compared with Fig. 1(a), it is clear that the as-cast Mg–12Gd–2Zn–0.5Nd–0.4Zr and Mg–12Gd–2Zn–1.0Nd–0.4Zr alloys show much finer and more uniform microstructures with the addition of Nd, as shown in Fig. 1(b) and (c). In addition, the morphologies of the eutectic phase do not change significantly, but its volume fraction increases slightly.

SEM images of the as-cast alloys and SFs are shown in Fig. 2. Table 1 shows the compositions of the α-Mg matrix (A1, B1, and C1), eutectic phase (A2, B2, and C2), and lamellar structure (A3, B3, and C3) in Fig. 2, which were analyzed by EDS, and the XRD patterns of the as-cast alloys are shown in Fig. 3. It can be seen from Fig. 2 that the eutectic phase is composed of α-Mg and β phases in alternating distribution, showing a fishbone shape. The gray lamellar structures are mostly distributed at the outer edge of the matrix grains, suggesting the formation of LPSO or SFs structures, as elliptically marked in Fig. 2(a), (c), and (e). The higher magnification SEM images shown in Fig. 2(b), (d) and (f) show clear lamellar structures at the outer edges of matrix grains near the eutectic phase. From the results of the EDS, Gd and Zn are mostly distributed in the eutectic phase of the alloys which is the same as the result in other Mg–RE alloys [38]. The contents of Gd and Zn in the lamellar area are less than those in the eutectic phase but higher as compared to those in the matrix. With the addition of Nd, the content of Gd in lamellar structures has an upward trend while the contents of Gd and Zn in the α-Mg matrix and eutectic phase have no significant changes. According to the results of XRD in Fig. 3, the β phase in the alloys is $(Mg,Zn)_3Gd$, and lamellar structures have no obvious diffraction peaks. It was reported that Nd mainly existed as MgZnNd in the Mg–Zn alloys [39]. However, the Mg alloys in this study do not appear obvious diffraction peaks of MgZnNd or other Nd-containing phases in the XRD results due to minor addition of Nd.

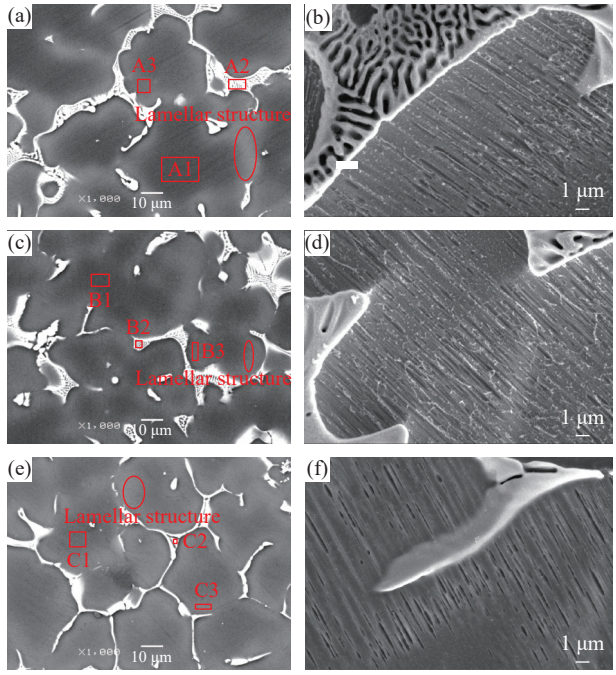

Fig. 2. SEM images of the as-cast alloys (left) and their lamellar structure (right): (a, b) Alloy 1; (c, d) Alloy 2; (e, f) Alloy 3.

Table 1. Chemical compositions of the marked areas in Fig. 2 wt%/at%

Alloy	Area	Gd	Zn	Zr	Nd	Mg
Alloy 1	A1	4.03/0.66	1.07/0.42	1.94/0.55	0	Bal.
	A2	37.20/9.15	8.65/5.12	0.37/0.16	0	Bal.
	A3	8.04/1.36	1.47/0.59	0.92/0.27	0	Bal.
Alloy 2	B1	5.88/0.98	1.14/0.46	0.79/0.23	1.00/0.18	Bal.
	B2	38.59/10.27	9.47/6.06	0.81/0.37	3.26/0.95	Bal.
	B3	12.28/2.15	1.31/0.55	0.29/0.09	0.47/0.09	Bal.
Alloy 3	C1	5.05/0.84	1.05/0.42	1.97/0.57	0.83/0.15	Bal.
	C2	36.05/9.41	10.29/6.46	0.67/0.30	4.03/1.15	Bal.
	C3	16.13/3.02	2.81/1.26	0.14/0.05	2.19/0.45	Bal.

In Table 1, the Nd content in lamellar structure is lower than that in the α-Mg matrix for Alloy 2, but the Nd content in lamellar structure is higher than that in the α-Mg matrix for Alloy 3. As the content of Nd increases, the volume fraction of eutectic phase increases. The Nd content in the eutectic phase also increases. Because lamellar structure are at the edge of the α-Mg matrix grains, connected with eutectic phase, the Nd content in the lamellar structure region also increases when the addition of Nd increases.

In order to determine whether the lamellar structure in the alloy is LPSO or SFs structure, TEM characterization was conducted on the alloys, and the image and corresponding selected area electron diffraction (SAED) pattern of the Mg–12Gd–2Zn–0.5Nd–0.4Zr alloy are shown in Fig. 4 as the representative. Based on the presence of strong streaks which were marked in Fig. 4 and the result of the SAED pattern, the lamellar structures are identified as SFs [23,40–41]. The primary condition for the formation of LPSO structure in Mg alloys is that the composition system of the alloy generally satisfies the condition of Mg–RE–TM (RE elements mainly include Gd, Y, La, Dy, Ho, Er, etc., and TM is a transition metal element, mainly including Cu, Zn, Ni, etc.) [42]. When Mg–RE–TM alloys satisfy some precondition in the process of solidification (such as certain temperature and cooling rate, disordered solid solution whose atomic ratio of RE and TM elements is close to a certain value), microstructure of al-

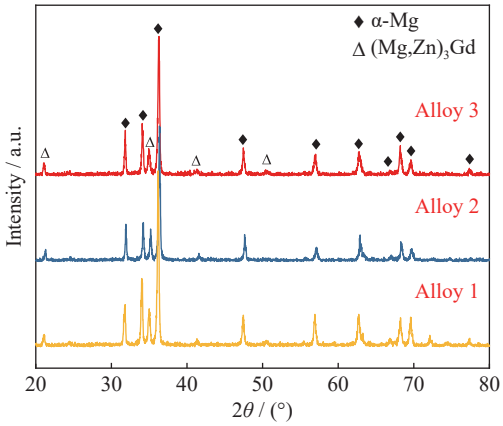

Fig. 3. XRD patterns of the as-cast alloys.

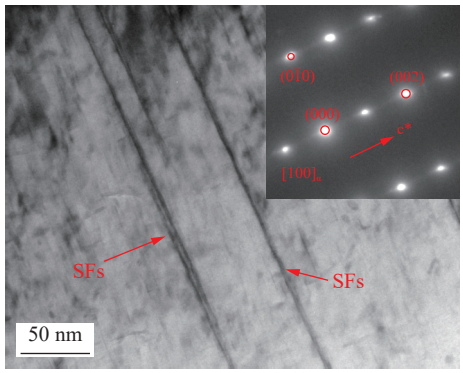

Fig. 4. TEM image of lamellar structures in Alloy 2 and the corresponding SAED pattern in the inset.

loys will undergo an orderly transformation, forming ordered solid solutions and thus presenting lamellar structures [43].

SFs [44–45] and LPSO [46–47] structures are often observed in extruded Mg–Gd–Zn–Zr alloys. They are lamellar structures with the same orientation in the same grain and different orientation in different grains. SFs are transformed into LPSO structures when the composition and stacking are ordered and certain thermodynamic and kinetic conditions are satisfied [48–49]. In this work, the result of TEM shows that the lamellar structures in the alloys are SFs which is rarely found in as-cast Mg alloys. It has been reported that the content of Zn in Mg–Gd–Zn series alloys has a great influence on the formation of LPSO structure [28]. The lamellar LPSO structure and SFs were both formed on $(0001)_{\alpha\text{-Mg}}$ habit plane and grown or extended along $[01\bar{1}0]_{\alpha\text{-Mg}}$ direction [30]. Adding Zn into Mg–Gd alloy can reduce the SF energy and LPSO may nucleate directly through SFs [28,30]. Moreover, it has been reported that the Zn/Gd mass ratio could affect the formation of LPSO structure. When the Zn/Gd atomic ratio is 0.4, the volume fraction of LPSO phase can reach the extreme value [50]. When the ratio deviates from 0.4, the volume fraction of LPSO decreases. The ratio of Zn/Gd is 0.16 in this study which is lower compared with 0.4, so the LPSO structure cannot be found. The relatively low content of Zn in this alloy leads to the low Zn/Gd mass ratio, and the SF energy is too high for SFs to form LPSO.

The grain size distribution of the Mg–12Gd–2Zn–*x*Nd–0.4Zr alloys is shown in Fig. 5. The average grain size of the alloy with 0wt% Nd is 56.6 μm, and that reduces to 29.0 μm and 25.8 μm with 0.5wt% and 1wt% Nd addition, respectively, indicating a good grain refinement caused by Nd. Moreover, the grain size distribution is more concentrated which means more uniform grains. For the RE-containing Mg alloys, the segregated RE elements gather at the solid–liquid interface where the crystal grows, thereby inhibiting the grain growth of the Mg alloys [51–52]. After adding Nd into the alloys, part of Nd is dissolved in the matrix, and the remaining is concentrated in eutectic phase. Nd is located at the solid–liquid interface during solidification and inhibits the growth of the grains, and thus further refines the grains and makes the microstructure uniform, as shown in Fig. 1.

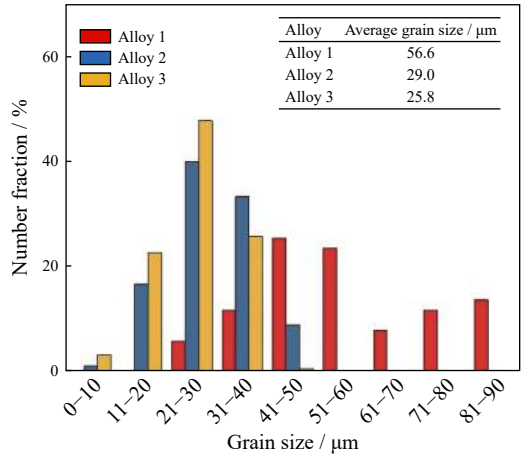

Alloy	Average grain size / μm
Alloy 1	56.6
Alloy 2	29.0
Alloy 3	25.8

Fig. 5. Grain size distribution of the as-cast alloys.

3.2. Mechanical properties

The tensile, compression, and the microhardness of the as-cast Mg–12Gd–2Zn–*x*Nd–0.4Zr alloys at room temperature are listed in Table 2. With the increasing addition of Nd, the TYS of the alloys increases, and TYS of Alloy 3 increases by 16.2% compared with that of Alloy 1. The ultimate tensile strength (UTS) of Alloy 2 (193 MPa) and Alloy 3 (194 MPa) are higher than that of Alloy 1 (172 MPa). The elongation (El.) of the alloys in tensile test shows slight improvement. The CYS presents a slight decrease with the addition of Nd, and the ultimate compression strength (UCS) of alloys is over 370 MPa. The elongation values of the alloys at room temperature in the compression test do not differ apparently which is in the range of 20.3% to 21.4%. CYS/TYS means the tension–compression asymmetry, and the CYS/TYS ratios of the three alloys are 1.30, 1.12, and 1.05, respectively, showing a decrease trend with the increase of Nd. Table 2 also shows the microhardness of the alloys. With the increase of Nd, the microhardness of the alloy increases slightly, which is similar to the trend of TYS.

The tensile fracture morphologies of the alloys are shown in Fig. 6. Some dimples and cleavage planes are observed in all the three alloys, indicating a mixed fracture with ductile and brittle characteristics. More dimples are visible by increasing Nd addition which suggests better plasticity. With the increase of Nd content, the volume fraction of the eutectic

Table 2. Mechanical properties of the Mg–12Gd–2Zn–*x*Nd–0.4Zr alloys

Alloy	Tension			Compression			CYS / TYS	Microhardness, HV
	TYS / MPa	UTS / MPa	El. / %	CYS / MPa	UCS / MPa	El. / %		
Alloy 1	142 ± 5	172 ± 2	2.4 ± 0.1	185 ± 2	377 ± 2	20.3 ± 0.2	1.30	70.7 ± 2.6
Alloy 2	158 ± 7	193 ± 4	2.7 ± 0.2	177 ± 4	384 ± 5	21.4 ± 0.5	1.12	78.3 ± 4.3
Alloy 3	165 ± 2	194 ± 3	3.4 ± 0.1	173 ± 4	397 ± 4	21.3 ± 0.4	1.05	80.9 ± 2.3

phase increases, which is harmful to the plasticity to some extent. However, the elongation of Alloy 2 and Alloy 3 is slightly improved. The improved elongation by increasing Nd is mainly due to the finer and homogeneous microstructures.

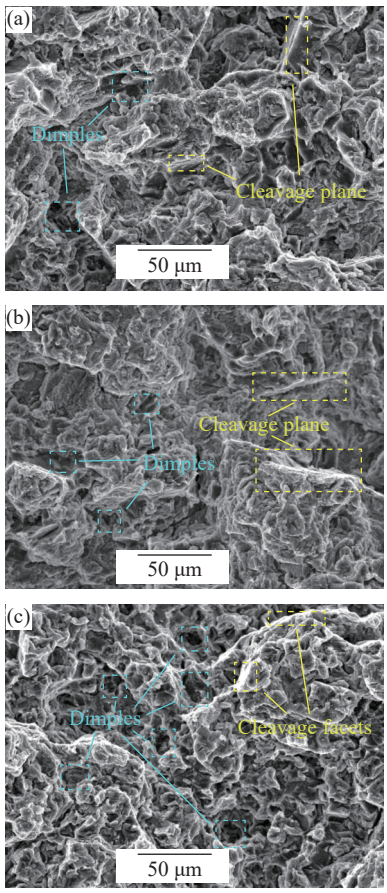

Fig. 6. Tensile fracture morphologies of the as-cast alloys: (a) Alloy 1; (b) Alloy 2; (c) Alloy 3.

The compression macroscopic fracture surface of the alloy is at a 45° angle to the axis of the sample, which has the characteristics of cutting off. It indicates that the alloy is fractured under shear deformation. Fig. 7 shows the compression fracture surfaces of the alloys. In general, the fracture morphologies are mainly composed of large cleavage planes. Microcracks near the eutectic phase are observed in Alloys 2 and 3.

To reveal the influence of the eutectic phase and SFs on the mechanical properties of the alloys, nanoindentation was used to measure the nanohardness of different phases. Fig. 8(a) shows the representative depths of indentations of α-Mg matrix, SFs area (since the width of the SF is only several nano shown in Fig. 4, the nano indentation test characterizes the nanohardness of the SFs aggregated area including partial α-Mg matrix but not the SFs themselves), and eutectic phase of the alloys. It can be seen that the depths are from high to low according to the order of α-Mg matrix, SFs, and eutectic phase. Moreover, with the increase of Nd addition, the depth of the α-Mg matrix is almost unchanged, but the depth of SFs, and eutectic phase becomes lower, indicating that the hardness increases. Fig. 8(b) shows the nanohardness of different areas (α-Mg matrix, SFs, and eutectic phase). The hardness of different phases increase according to the sequence of α-Mg matrix, SFs, and eutectic phase. The nanohardness of α-Mg matrix in Alloys 1, 2, and 3 are 0.78, 0.78, and 0.77 GPa, respectively, which suggests that the addition of Nd has little effect on the nanohardness of the matrix. However, the nanohardness of SFs are 0.93, 1.15, and 1.22 GPa, and that of eutectic phase are 1.27, 1.34, and 1.40 GPa for Alloys 1, 2, and 3, respectively, which means that the nanohardness of the SFs and eutectic phase increase with the increasing addition of Nd.

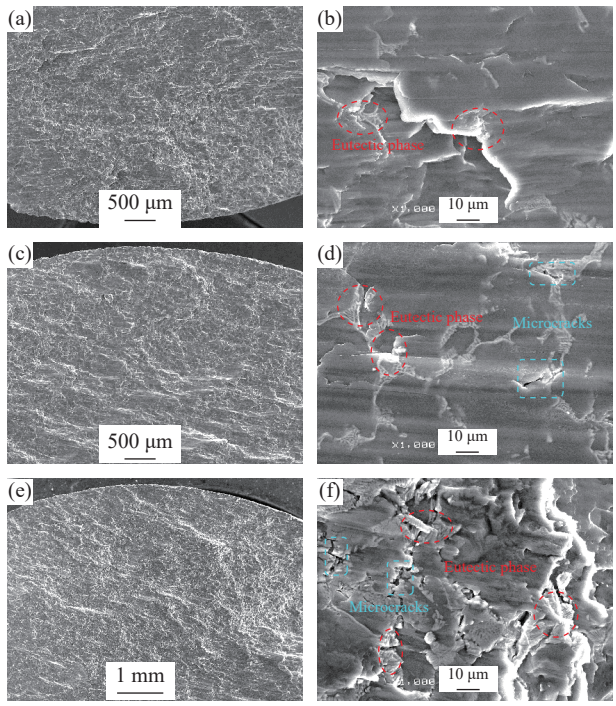

Fig. 7. Compression fracture morphologies of the as-cast alloys (a, b) Alloy 1, (c, d) Alloy 2, (e, f) Alloy 3.

For plastic deformation of Mg alloys, SFs with different orientations in different grains can play a role in preventing dislocation movement and effectively improving the elongation and tensile strength of the alloys [53]. In Fig. 8(b), it can be found that with the increase of Nd content, the nanohardness of α-Mg matrix hardly changes, while it increases significantly at SFs. The addition of Nd may increase the volume

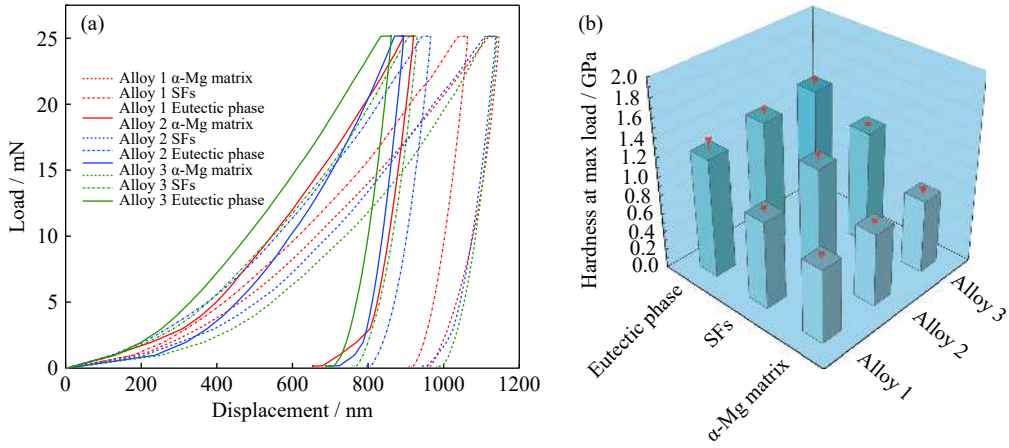

Fig. 8. Nanohardness load-displacement curves (a) and values (b) of different phases in the alloys.

fraction of SFs, and lead to the improvement of strength.

The nanohardness of the α-Mg matrix is almost unchanged, which is attributed to no obvious increase of solute atoms under as-cast condition. The nanohardness of the SFs is significantly improved. According to the analysis of the compositions by EDS, it may be caused by increasing Gd and Nd content in SFs area. And the nanohardness of the eutectic phase has a slight upward trend due to higher Nd concentration. The nanohardness value of the eutectic phase in the alloys was the highest, followed by that of the SFs and the α-Mg matrix. SFs and eutectic phase have the higher nanohardness calculated from the unloading curves, which is attributed to higher RE and Zn contents [42]. The higher hardness of SFs and eutectic phases are also the factors for the improved TYS and microhardness of the alloys besides grain refinement and solution strengthening.

As can be seen from Table 2, the elongation and TYS of the alloys were improved by adding Nd element. Nd distributes in α-Mg matrix, SFs, and eutectic phase. As solute atoms, Nd atoms cause lattice distortion which hinder dislocation movement and make slip difficult, thus playing a role of solid solution strengthening. Grain size is also one of the important factors affecting the mechanical properties of the alloy [54–55]. The grain size of the alloy decreases apparently by increasing Nd addition, which leads to the increase of both tensile strength and elongation of the alloy. Alloy 3 exhibits the highest TYS and elongation mainly due to solution strengthening and grain refinement strengthening.

The UCS value of the alloys is over 370 MPa, which is almost twice than the UTS of the alloys. In addition, the elongation of the alloys reaches over 20% in the compression experiment, which is greatly improved compared with the elongation of tension. This is mainly due to the different deformation mechanisms of Mg alloys in tensile and compression tests. In the tensile test, the deformation mechanism of the alloys is mainly basal slip, which is hindered by dislocations and grain boundaries. In compression tests, the alloys were cut off at an angle of 45°. According to the Mohr-Coulomb criterion [56], the shear stress at the oblique section of the alloys reaches its limit under the action of pressure load. During the test, the cracks which were generated in the deformation extend to the whole cross section. During compression, the friction force related to the compression stress will be generated in the alloys to prevent the section from sliding, so the crack tip is not easy to expand. The friction in this process is more effective than the hindrance in tensile testing. Therefore, the UCS and the elongation under compression are much higher than those of the tensile test.

The increased Nd content makes the grain size of Alloys 2 and 3 decrease and the microstructure more uniform, as shown in Fig. 5. However, CYS showed a slight decrease as Nd addition increases, which is different from the results of TYS. In Mg alloys, as two dominant deformation mechanisms, slip and twinning are easily activated during tension or compression test [57]. It was found that the grain size effect on twinning is much stronger than that on slip in Mg alloys according to Hall-Petch theory [58–59]. Therefore, with the decrease of grain size, twinning is more difficult to activate [31]. In the present study, no twinnings were found in the compression test. So here it is suggested that slip is the main mechanism of deformation for the alloys. At room temperature, basel slip often occurs in the tensile process of Mg alloys, while non-basel slip often occurs in compression [60]. The slip systems are different, which means that the fine grains does not mean the increase of CYS. In addition, the homogeneous microstructure resulted in reduction in mechanical anisotropy of Alloys 2 and 3. Therefore, the CYS of Alloy 1 may be larger than the normal value due to its anisotropy. Moreover, the CYS of Alloys 2 and 3 decrease slightly because of uniform microstructure and decrease in anisotropy. So the CYS of Alloys 2 and 3 show a slight decrease trend as compared to that of Alloy 1.

In the tension–compression experiments, the CYS of Alloy 1 is greater than that of the TYS, and its ratio (CYS/TYS) is 1.30, which shows an obvious tension–compression yield asymmetry in reverse [32]. With the increase of Nd content, the ratio (CYS/TYS) of Alloy 2 is 1.12 and that of Alloy 3 is 1.05. This indicates that the tension–compression yield asymmetry in reverse of the alloy decreases significantly, and the mechanical properties of Alloy 3 are more stable than those of Alloys 1 and 2. It has been reported that finer and more homogeneous microstructure is beneficial to decrease

tension–compression asymmetry [31]. So the reduced tension–compression asymmetry in reverse is mainly affected by the finer and more homogenous microstructure which is caused by the increase of Nd content.

4. Conclusions

(1) The as-cast Mg–12Gd–2Zn–*x*Nd–0.4Zr alloys mainly consist of α-Mg matrix, eutectic phase, and SFs. After adding Nd into the alloy, the microstructure is refined and homogenized, and the volume fraction of the eutectic phase increases.

(2) The TYS, microhardness, and elongation of the alloys are increased with increasing Nd addition. Moreover, the nanohardness of the SFs and eutectic phases are both improved as Nd content increases.

(3) Mg–12Gd–2Zn–0.4Zr alloy shows an obvious tension–compression yield asymmetry in reverse with the data of 1.30. With increasing Nd addition, the asymmetry in reverse of the alloys shows a remarkable decrease from 1.30 to 1.12 and 1.05. The alloy with 1wt% Nd addition exhibits the best compressive mechanical properties.

Acknowledgements

This work was financially supported by the National Natural Science Foundation of China (No. 52071175), the Natural Science Foundation of Higher Education Institutions of Jiangsu Province - Key Project, China (No. 18KJA430008), the Key Research & Development Plan (Social Development) of Jiangsu Province, China (No. BE2020702), and the Postgraduate Research & Practice Innovation Program of Jiangsu Province (No. SJCX21_0923).

Conflict of Interest

The authors have no conflicts to declare.

References

[1] Y.X. Li, C.L. Yang, X.Q. Zeng, P.P. Jin, D. Qiu, and W.J. Ding, Microstructure evolution and mechanical properties of magnesium alloys containing long period stacking ordered phase, *Mater. Charact.*, 141(2018), p. 286.

[2] D.K. Xu, E.H. Han, and Y.B. Xu, Effect of long-period stacking ordered phase on microstructure, mechanical property and corrosion resistance of Mg alloys: A review, *Prog. Nat. Sci. Mater. Int.*, 26(2016), No. 2, p. 117.

[3] Q.Z. Liu, X.F. Ding, Y.P. Liu, and X.J. Wei, Analysis on micro-structure and mechanical properties of Mg–Gd–Y–Nd–Zr alloy and its reinforcement mechanism, *J. Alloys Compd.*, 690(2017), p. 961.

[4] J.S. Xie, J.H. Zhang, Z.H. You, *et al*., Towards developing Mg alloys with simultaneously improved strength and corrosion resistance via RE alloying, *J. Magnes. Alloys*, 9(2021), No. 1, p. 41.

[5] A.M. Majd, M. Farzinfar, M. Pashakhanlou, and M.J. Nayyeri, Effect of RE elements on the microstructural and mechanical properties of as-cast and age hardening processed Mg–4Al–2Sn alloy, *J. Magnes. Alloys*, 6(2018), No. 3, p. 309.

[6] Z. Zhang, J.H. Zhang, J. Wang, *et al*., Toward the development of Mg alloys with simultaneously improved strength and ductility by refining grain size via the deformation process, *Int. J. Miner. Metall. Mater.*, 28(2021), No. 1, p. 30.

[7] S.J. Wang, Z. Han, Y.J. Nie, *et al*., Modified mechanical properties of Mg–Nd–Zn–Ag–Zr alloy by solution treatment for cardiovascular stent application, *Mater. Res. Express*, 6(2019), No. 8, art. No. 085416.

[8] W.B. Luo, Z.Y. Xue, and W.M. Mao, Effect of heat treatment on the microstructure and micromechanical properties of the rapidly solidified $Mg_{61.7}Zn_{34}Gd_{4.3}$ alloy containing icosahedral phase, *Int. J. Miner. Metall. Mater.*, 26(2019), No. 7, p. 869.

[9] J.X. Chen, L.L. Tan, I.P. Etim, and K. Yang, Comparative study of the effect of Nd and Y content on the mechanical and biodegradable properties of Mg–Zn–Zr–*x*Nd/Y (x = 0.5, 1, 2) alloys, *Mater. Technol.*, 33(2018), No. 10, p. 659.

[10] L.K. Singh, A. Bhadauria, A. Srinivasan, U.T.S. Pillai, and B.C. Pai, Effects of gadolinium addition on the microstructure and mechanical properties of Mg–9Al alloy, *Int. J. Miner. Metall. Mater.*, 24(2017), No. 8, p. 901.

[11] X.B. Zhang, J.W. Dai, Q.S. Dong, Z.X. Ba, and Y.J. Wu, Corrosion behavior and mechanical degradation of as-extruded Mg–Gd–Zn–Zr alloys for orthopedic application, *J. Biomed. Mater. Res. Part B*, 108(2020), No. 3, p. 698.

[12] Y. Kawamura, K. Hayashi, A. Inoue, and T. Masumoto, Rapidly solidified powder metallurgy $Mg_{97}Zn_1Y_2$ alloys with excellent tensile yield strength above 600 MPa, *Mater. Trans.*, 42(2001), No. 7, p. 1172.

[13] A. Inoue, Y. Kawamura, M. Matsushita, K. Hayashi, and J. Koike, Novel hexagonal structure and ultrahigh strength of magnesium solid solution in the Mg–Zn–Y system, *J. Mater. Res.*, 16(2001), No. 7, p. 1894.

[14] Y.H. Zhang, Y.Q. Li, W. Zhang, *et al*., Gaseous hydrogen storage properties of Mg–Y–Ni–Cu alloys prepared by melt spinning, *J. Rare Earths*, 37(2019), No. 7, p. 750.

[15] Z.W. Geng, D.H. Xiao, and L. Chen, Microstructure, mechanical properties, and corrosion behavior of degradable Mg–Al–Cu–Zn–Gd alloys, *J. Alloys Compd.*, 686(2016), p. 145.

[16] Z.B. Ding, Y.H. Zhao, R.P. Lu, *et al*., Effect of Zn addition on microstructure and mechanical properties of cast Mg–Gd–Y–Zr alloys, *Trans. Nonferrous Met. Soc. China*, 29(2019), No. 4, p. 722.

[17] S.J. Ouyang, W.C. Liu, G.H. Wu, *et al*., Microstructure and mechanical properties of as-cast Mg–8Li–*x*Zn–*y*Gd (x = 1, 2, 3, 4; y = 1, 2) alloys, *Trans. Nonferrous Met. Soc. China*, 29(2019), No. 6, p. 1211.

[18] K. Hagihara, Z.X. Li, M. Yamasaki, Y. Kawamura, and T. Nakano, Strengthening mechanisms acting in extruded Mg-based long-period stacking ordered (LPSO)-phase alloys, *Acta Mater.*, 163(2019), p. 226.

[19] N. Tahreen, D.F. Zhang, F.S. Pan, X.Q. Jiang, D.Y. Li, and D.L. Chen, Strengthening mechanisms in magnesium alloys containing ternary I, W and LPSO phases, *J. Mater. Sci. Technol.*, 34(2018), No. 7, p. 1110.

[20] J.W. Dai, X.B. Zhang, Y. Fei, Z.Z. Wang, and H.M. Sui, Effect of solution treatment on microstructure and corrosion properties of Mg–4Gd–1Y–1Zn–0.5Ca–1Zr alloy, *Acta Metall. Sinica Engl. Lett.*, 31(2018), No. 8, p. 865.

[21] Z.Y. Xue, Y.J. Ren, W.B. Luo, Y. Ren, P. Xu, and C. Xu, Microstructure evolution and mechanical properties of a large-sized ingot of Mg−9Gd−3Y−1.5Zn−0.5Zr (wt%) alloy after a lower-temperature homogenization treatment, *Int. J. Miner. Metall. Mater.*, 24(2017), No. 3, p. 271.

[22] C. Xu, J.H. Zhang, S.J. Liu, *et al*., Microstructure, mechanical and damping properties of Mg–Er–Gd–Zn alloy reinforced with stacking faults, *Mater. Des.*, 79(2015), p. 53.

[23] Y. Feng, J.H. Zhang, P.F. Qin, *et al*., Characterization of elevated-temperature high strength and decent thermal conductivity extruded Mg–Er–Y–Zn alloy containing nano-spaced stacking faults, *Mater. Charact.*, 155(2019), art. No. 109823.

[24] L. Zhang, J.H. Zhang, C. Xu, Y.B. Jing, J.P. Zhuang, R.Z. Wu,

and M.L. Zhang, Formation of stacking faults for improving the performance of biodegradable Mg–Ho–Zn alloy, *Mater. Lett.*, 133(2014), p. 158.

[25] H.J. Si, Y.X. Jiang, Y. Tang, and L.J. Zhang, Stable and metastable phase equilibria in binary Mg–Gd system: A comprehensive understanding aided by CALPHAD modeling, *J. Magnes. Alloys*, 7(2019), No. 3, p. 501.

[26] X.B. Zhang, Z.X. Ba, Z.Z. Wang, Y.J. Wu, and Y.J. Xue, Effect of LPSO structure on mechanical properties and corrosion behavior of as-extruded GZ51K magnesium alloy, *Mater. Lett.*, 163(2016), p. 250.

[27] X.G. Zhang, L.G. Meng, C.F. Fang, P. Peng, F. Ja, and H. Hao, Effect of Nd on the microstructure and mechanical properties of Mg–8Gd–5Y–2Zn–0.5Zr alloy, *Mater. Sci. Eng. A*, 586(2013), p. 19.

[28] Z.B. Ding, R.P. Lu, Y.H. Zhao, *et al*., The microstructure and mechanical properties of As-cast Mg–10Gd–3Y–*x*Zn–0.6Zr (*x* = 0, 0.5, 1 and 2 wt%) alloys, *Mater. Res.*, 21(2018), No. 5, art. No. e20170992.

[29] M. Li, K. Zhang, Z.W. Du, X.G. Li, and M.L. Ma, Microstructure evolution and mechanical properties of Mg–7Gd–3Y–1Nd–1Zn–0.5Zr alloy, *Trans. Nonferrous Met. Soc. China*, 26(2016), No. 7, p. 1835.

[30] F.S. Pan, S.Q. Luo, A.T. Tang, J. Peng, and Y. Lu, Influence of stacking fault energy on formation of long period stacking ordered structures in Mg–Zn–Y–Zr alloys, *Prog. Nat. Sci.: Mater. Int.*, 21(2011), No. 6, p. 485.

[31] S. Kamrani and C. Fleck, Effects of calcium and rare-earth elements on the microstructure and tension–compression yield asymmetry of ZEK100 alloy, *Mater. Sci. Eng. A*, 618(2014), p. 238.

[32] E. Dogan, I. Karaman, G. Ayoub, and G. Kridli, Reduction in tension–compression asymmetry via grain refinement and texture design in Mg–3Al–1Zn sheets, *Mater. Sci. Eng. A*, 610(2014), p. 220.

[33] S.H. Park, J.H. Lee, B.G. Moon, and B.S. You, Tension–compression yield asymmetry in as-cast magnesium alloy, *J. Alloys Compd.*, 617(2014), p. 277.

[34] Y. Jiang, Y.A. Chen, and Y. Wang, Compound role of tension twins and compression twins in microstructure and mechanical properties of Mg–Sn–Li rod, *Mater. Sci. Eng. A*, 682(2017), p. 31.

[35] X.Y. Xu, X.H. Chen, W.W. Du, Y.X. Geng, and F.S. Pan, Effect of Nd on microstructure and mechanical properties of as-extruded Mg–Y–Zr–Nd alloy, *J. Mater. Sci. Technol.*, 33(2017), No. 9, p. 926.

[36] G.S. Hu, D.F. Zhang, T. Tang, *et al*., Effects of Nd addition on microstructure and mechanical properties of Mg–6Zn–1Mn–4Sn alloy, *Mater. Sci. Eng. A*, 634(2015), p. 5.

[37] X. Liu, Z.Q. Zhang, Q.C. Le, and L. Bao, Effects of Nd/Gd value on the microstructures and mechanical properties of Mg–Gd–Y–Nd–Zr alloys, *J. Magnes. Alloys*, 4(2016), No. 3, p. 214.

[38] X. Zhang, J. Dai, H. Yang, S. Liu, X. He, and Z. Wang, Influence of Gd and Ca on microstructure, mechanical and corrosion properties of Mg–Gd–Zn(–Ca) alloys, *Mater. Technol.*, 32(2017), No. 7, p. 399.

[39] H. Zengin and Y. Turen, Effect of Y addition on microstructure and corrosion behavior of extruded Mg-Zn–Nd–Zr alloy, *J. Magnes. Alloys*, 8(2020), No. 3, p. 640.

[40] K. Matsubara, H. Kimizuka, and S. Ogata, Formation of $\{11\bar{2}1\}$ twins from I_1-type stacking faults in Mg: A molecular dynamics study, *Comput. Mater. Sci.*, 122(2016), p. 314.

[41] B.L. Yin, Z.X. Wu, and W.A. Curtin, First-principles calculations of stacking fault energies in Mg–Y, Mg–Al and Mg–Zn alloys and implications for <c + a> activity, *Acta Mater.*, 136(2017), p. 249.

[42] Y.X. Du, Y.J. Wu, L.M. Peng, J. Chen, X.Q. Zeng, and W.J. Ding, Formation of lamellar phase with 18R-type LPSO structure in an as-cast $Mg_{96}Gd_3Zn_1$(at%) alloy, *Mater. Lett.*, 169(2016), p. 168.

[43] Y.J. Wu, D.L. Lin, X.Q. Zeng, L.M. Peng, and W.J. Ding, Formation of a lamellar 14H-type long period stacking ordered structure in an as-cast Mg–Gd–Zn–Zr alloy, *J. Mater. Sci.*, 44(2009), No. 6, p. 1607.

[44] X. Zhang, S.K. Kairy, J. Dai, and N. Birbilis, A closer look at the role of nanometer scale solute-rich stacking faults in the localized corrosion of a magnesium alloy GZ31K, *J. Electrochem. Soc.*, 165(2018), No. 7, p. C310.

[45] X.B. Zhang, J.W. Dai, R.F. Zhang, Z.X. Ba, and N. Birbilis, Corrosion behavior of Mg–3Gd–1Zn–0.4Zr alloy with and without stacking faults, *J. Magnes. Alloys*, 7(2019), No. 2, p. 240.

[46] S.Q. Yin, Z.Q. Zhang, X. Liu, *et al*., Effects of Zn/Gd ratio on the microstructures and mechanical properties of Mg–Zn–Gd–Zr alloys, *Mater. Sci. Eng. A*, 695(2017), p. 135.

[47] X.M. Zong, D. Wang, W. Liu, K.B. Nie, C.X. Xu, and J.S. Zhang, Effect of precipitated phases on corrosion of $Mg_{95.8}Gd_3Zn_1Zr_{0.2}$ alloy with long-period stacking ordered structure, *Acta Metall. Sinica Engl. Lett.*, 29(2016), No. 1, p. 32.

[48] Y.J. Wu, X.Q. Zeng, D.L. Lin, L.M. Peng, and W.J. Ding, The microstructure evolution with lamellar 14H-type LPSO structure in an $Mg_{96.5}Gd_{2.5}Zn_1$ alloy during solid solution heat treatment at 773 K, *J. Alloys Compd.*, 477(2009), No. 1-2, p. 193.

[49] W.J. Ding, Y.J. Wu, L.M. Peng, X.Q. Zeng, G.Y. Yuan, and D.L. Lin, Formation of 14H-type long period stacking ordered structure in the as-cast and solid solution treated Mg–Gd–Zn–Zr alloys, *J. Mater. Res.*, 24(2009), No. 5, p. 1842.

[50] J.Y. Zhang, M. Xu, X.Y. Teng, and M. Zuo, Effect of Gd addition on microstructure and corrosion behaviors of Mg–Zn–Y alloy, *J. Magnes. Alloys*, 4(2016), No. 4, p. 319.

[51] J. Wei, Q.D. Wang, L. Zhang, *et al*., Microstructure refinement of Mg–Al–RE alloy by Gd addition, *Mater. Lett.*, 246(2019), p. 125.

[52] X.Y. Hu, P.H. Fu, D. StJohn, L.M. Peng, M. Sun, and M.X. Zhang, On grain coarsening and refining of the Mg–3Al alloy by Sm, *J. Alloys Compd.*, 663(2016), p. 387.

[53] K. Wei, L.R. Xiao, B. Gao, *et al*., Enhancing the strain hardening and ductility of Mg–Y alloy by introducing stacking faults, *J. Magnes. Alloys*, 8(2020), No. 4, p. 1221.

[54] J.H. He, L. Jin, F.H. Wang, S. Dong, and J. Dong, Mechanical properties of Mg–8Gd–3Y–0.5Zr alloy with bimodal grain size distributions, *J. Magnes. Alloys*, 5(2017), No. 4, p. 423.

[55] S. Lv, F.Z. Meng, X.L. Lu, *et al*., Influence of Nd addition on microstructures and mechanical properties of a hot-extruded Mg−6.0Zn−0.5Zr (wt.%) alloy, *J. Alloys Compd.*, 806(2019), p. 1166.

[56] P. Papanastasiou and D. Durban, Singular crack-tip plastic fields in Tresca and Mohr-Coulomb solids, *Int. J. Solids Struct.*, 136-137(2018), p. 250.

[57] Q.H. Wang, Y. Song, B. Jiang, *et al*., Fabrication of Mg/Mg composite with sleeve-core structure and its effect on room-temperature yield asymmetry via bimetal casting-co-extrusion, *Mater. Sci. Eng. A*, 769(2020), art. No. 138476.

[58] L.B. Tong, M.Y. Zheng, S. Kamado, *et al*., Reducing the tension–compression yield asymmetry of extruded Mg–Zn–Ca alloy via equal channel angular pressing, *J. Magnes. Alloys*, 3(2015), No. 4, p. 302.

[59] H.H. Yu, Y.C. Xin, M.Y. Wang, and Q. Liu, Hall-Petch relationship in Mg alloys: A review, *J. Mater. Sci. Technol.*, 34(2018), No. 2, p. 248.

[60] Y.Q. Chi, X.H. Zhou, X.G. Qiao, H.G. Brokmeier, and M.Y. Zheng, Tension–compression asymmetry of extruded Mg–Gd–Y–Zr alloy with a bimodal microstructure studied by *in situ* synchrotron diffraction, *Mater. Des.*, 170(2019), art. No. 107705.